Detection and Identification of Transient Intermediates in the Reactions of Tryptophan Synthase with Oxindolyl-L-alanine and 2,3-Dihydro-L-tryptophan. Evidence for a Tetrahedral (*gem*-Diamine) Intermediate†

Melinda Roy,‡ Edith W. Miles,§ Robert S. Phillips,∥ and Michael F. Dunn*,‡

Department of Biochemistry, University of California at Riverside, Riverside, California 92521, Section on Pharmacology, Laboratory of Biochemical Pharmacology, National Institutes of Health, Bethesda, Maryland 20892, and Departments of Chemistry and Biochemistry, University of Georgia, Athens, Georgia 30602

Received April 21, 1988; Revised Manuscript Received July 18, 1988

ABSTRACT: The reactions of 2,3-dihydro-L-tryptophan (DHT) and oxindolyl-L-alanine (OXA) with tryptophan synthase have been investigated by rapid-scanning stopped-flow (RSSF) spectroscopy and by the concentration dependence of rates measured by single-wavelength stopped-flow (SWSF) spectroscopy. The RSSF spectral changes for DHT and OXA show the disappearance of the internal aldimine (λ_{max} 412 nm), the formation and decay of intermediates absorbing ≤340 nm, and the appearance of the quinonoid (λ_{max} 492 and 480 nm, respectively). Rate constants determined by SWSF were either well resolved (i.e., k_1[DHT], $k_{-1} > k_2$, $k_{-2} > k_3$, k_{-3}) or indicative of a tightly coupled system (i.e., k_1[OXA], $k_{-1} \geq k_2$, $k_{-2} > k_3$, k_{-3}). The RSSF spectral changes and SWSF kinetic studies together with computer simulations of the kinetic time courses are consistent with a mechanism that includes formation of a bleached species. Detection of these shorter wavelength species in the reactions of OXA and DHT indicates that substrate analogues with tetrahedral geometry at C-3 induce new protein–substrate interactions that result in the accumulation of species not previously detected in the tryptophan synthase system. The bleached species with λ_{max} ≤340 nm are proposed as the *gem*-diamine intermediates.

The pyridoxal phosphate (PLP)[1] requiring β subunits of the $\alpha_2\beta_2$ complex of tryptophan synthase (EC 4.1.2.20) from *Escherichia coli* catalyze the replacement of the β-hydroxyl group of L-serine with indole to yield L-tryptophan and water (Miles, 1979). The distinctive UV–visible spectral properties of the PLP moiety provide a sensitive probe for the detection and identification of intermediates formed in the reactions of the β subunit.

It has been proposed that an indolenine derivative (I) of the L-Trp quinonoid is an intermediate both in the synthesis of L-Trp (Lane & Kirschner, 1983; Phillips et al., 1984; Drewe & Dunn, 1986) and in the degradation of L-Trp by tryptophanase (Davis & Metzler, 1972).

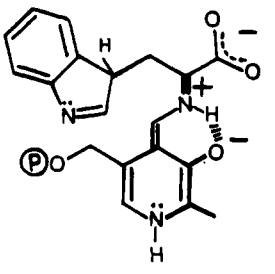

I

In support of this proposal, it has been shown that the L-Trp derivatives (αS,3*S*)-2,3-dihydrotryptophan (DHT) and oxindolyl-L-alanine (OXA) are potent, slow-binding, and relatively tight binding inhibitors, presumably because they form reaction-intermediate analogues of I (Phillips et al., 1984, 1985). Like the proposed indolenine intermediate, these analogues

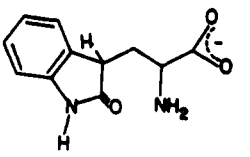

OXA

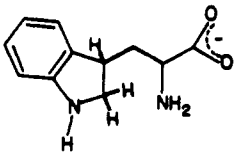

DHT

have sp^3 hybridization (tetrahedral geometry) at C-3 of the heterocyclic indole ring. Addition of OXA or DHT to solutions of tryptophan synthase results in new absorption bands at 480 and 494 nm, respectively, which are ascribed to quinonoid intermediates (Phillips et al., 1984).

In this paper, we report the formation and decay of intermediates in the reactions of $\alpha_2\beta_2$ with OXA and DHT, respectively, via rapid-scanning stopped-flow (RSSF) UV–visible spectroscopy. We have followed the concentration dependencies of these relaxations via conventional single-wavelength stopped-flow (SWSF) spectroscopy. Spectral data and kinetic analyses indicate the presence of bleached intermediates (with λ_{max} <325 nm) in the reactions of both analogues. Computer simulations of the kinetic time courses are consistent with mechanisms that include *gem*-diamine species as bleached intermediates. Inhibition by DHT and OXA is principally due to the accumulation of these species.

Materials and Methods

Instrumentation. Routine UV–visible spectra were obtained with a Hewlett-Packard 8450A spectrophotometer. Single-wavelength transient kinetic studies were performed with a Durrum Model D110 stopped-flow spectrophotometer interfaced for on-line computer data acquisition and analysis (Dunn et al., 1979). Rapid-scanning stopped-flow spectroscopy was

† This work was supported by Research Grants DMB-8703697 and PCM 84-8513 from the National Science Foundation.

‡ University of California at Riverside.

§ National Institutes of Health.

∥ University of Georgia.

[1] Abbreviations: PLP, pyridoxal 5′-phosphate; $\alpha_2\beta_2$, the native form of *E. coli* tryptophan synthase; OXA, oxindolyl-L-alanine; DHT, (αS,3*S*)-2,3-dihydrotryptophan.

0006-2960/88/0427-8661$01.50/0

carried out on a modified Durrum Model D110 stopped-flow spectrophotometer interfaced with a Princeton Applied Research 1218 controller and 1214 photodiode array detector (Dunn et al., 1982; Koerber et al., 1983). The timing sequence was 8.605, 17, 26, 34, 95, 120, 510, and 920 ms and 1.97, 4.1, 6.3, 9.3, 11.9, 14.5, 17, 34, and 69 s. The concentrations reported refer to conditions after mixing.

Materials. OXA was prepared by oxidation of L-Trp, as described earlier (Phillips et al., 1984), and (3*S*)-DHT was synthesized from the reduction of L-Trp with pyridine–borane complex in trifluoroacetic acid and resolved into the (3*R*) and (3*S*) isomers by preparative HPLC (Phillips et al., 1985). Deuteriated (3*S*)-DHT was prepared by reduction of [α-^{2}H]-L-Trp, which was obtained from the deuteriation of L-Ser in the tryptophan synthase catalyzed condensation of indole and L-Ser in ^2H_2O (Turner et al., 1985). The reaction mixture contained 10 mM L-Ser, 4 mM indole, and 40 μM $\alpha_2\beta_2$ in 0.1 M Tris-^{2}HCl, pH* 8.0, made up in ^2H_2O. The resulting [α-^{2}H]-L-Trp was separated from the enzyme and the excess L-Ser on a column of Sephadex G-25 superfine, in a modification of the procedure described for purification of 6-azido-L-Trp (Miles & Phillips, 1985). The ^{2}H content at the α position was assayed as $\geq$95% by ^{1}H NMR integration.

All other chemicals were purchased from Sigma (reagent grade) and used without further purification. Purification of *E. coli* tryptophan synthase, measurement of enzymatic activity, and determination of protein concentrations were carried out as described by Drewe and Dunn (1985) and Drewe (1984).

Computer Simulations. The RUNGE chemical simulation program from Anarac Associates was used to test mechanistic hypotheses. Differential rate equations for elementary chemical reactions give reactant concentrations over time. RUNGE used a fourth-order Runge–Kutta approximation to calculate the theoretical time course of each species in a complex chemical reaction. The concentration of all species can be calculated over time.

RESULTS

Rapid-Scanning Stopped-Flow Studies. The transient UV–visible spectral changes that occur in the reaction of tryptophan synthase and DHT are shown in Figure 1A. These RSSF data present time-resolved spectral changes showing the decrease of the internal aldimine (λ_{max} 412 nm) and the appearance of a new species (λ_{max} 492 nm). The accompanying single-wavelength time courses (insets to Figure 1A) demonstrate the formation and decay of an intermediate with $\lambda_{max} \leq$340 nm, the decay of the 412-nm band, and the increase of the 492-nm band. The relative intensities of the spectral bands and the lack of a clean isoabsorbance point at 460 nm indicate the accumulation of an intermediate with an absorption maximum other than 340 or 492 nm. The extinction coefficient for the 412-nm band of the internal aldimine is about 6000 M^{-1} cm^{-1} (on the basis of comparisons to free PLP in 0.1 N NaOH, 0.1 N HCl, and pH 7.8 buffer), while the extinction coefficients for tryptophan synthase quinonoidal intermediates appear to be 5–10 times greater (depending on the substrate) (Miles, 1979, 1986; Dunn et al., 1987a,b). It appears that at equilibrium a majority of the enzyme is in the form of one or more species with λ_{max} <320 nm.

Equilibrium difference absorption spectra show that the addition of (3*S*)-2,3-H_2-5-fluoro-Trp to $\alpha_2\beta_2$ results in an increase at 325 nm (Miles et al., 1986), also indicating a shorter wavelength intermediate. Correspondingly, difference spectra derived from the RSSF data (see Figure 1B) reveal an increase in absorbance at ~312 nm and below. Due to the sensitivity limitation of our RSSF detector, spectra become increasingly noisy as the λ becomes shorter. Therefore, the actual λ_{max} for this UV increase may be located well below 312 nm. Due to the limitations of the sensitivity of our RSSF detector in this wavelength region and to the large absorbancies below 300 nm, we have not been able to determine the exact nature of the spectral changes at these shorter wavelengths. The time course at 312 nm from the RSSF data has been plotted and is shown in the inset to Figure 1B. The rate of increase at 312 nm is faster than the rate of increase at 492 nm (compare inset d of Figure 1A with the inset to Figure 1B). Consequently, the 312-nm spectral changes must arise from a different intermediate and, therefore, cannot be due to a second electronic transition of the 492-nm spectral band.

The RSSF data for the reaction of tryptophan synthase with OXA are presented in Figure 2. Here the time-resolved spectral changes show the disappearance of the 412-nm spectral band of the internal aldimine and the appearance of new spectral bands at 325, and 480, and ~445 nm (cf. Figure 1A). Since there is not a clean isoabsorbance point (viz., the time course at 443 nm in the inset to Figure 2), the decay of the 412-nm internal aldimine and the formation of the 480-nm quinoidal intermediate are not concomitant processes. The insets to Figure 2 compare the increases in absorbance at both 325 and 480 nm with the decrease at 412 nm and the changes at 443 nm. These time courses establish that the spectral band at 325 nm appears more rapidly than does the band at 480 nm.

Single-Wavelength Studies. The contention that intermediates with $\lambda_{max} \leq$325 nm accumulate in the reactions of both OXA and DHT with tryptophan synthase is supported by single-wavelength stopped-flow time courses measured at different substrate concentrations. The time course of the reaction of DHT with $\alpha_2\beta_2$ was investigated at 412, 492, and 340 nm with DHT concentrations after mixing ranging from 0.2 to 4.0 mM. The observed kinetic relaxations were determined by computer fitting of the time courses to eq 1,

$$A_t = A_\infty \pm \sum_{i=1}^{3} A_j \exp(-t/\tau_j) \quad (1)$$

where A_t is the absorbance at time t, A_∞ is the absorbance at t_∞, A_j is the amplitude of the jth relaxation (τ_j). For example, the time course at 492 nm (see the inset to Figure 1A) was found to be adequately fit when $j = 1$; consequently, the changes at this wavelength are described by a single relaxation. Three relaxations each were required to fit the time courses at 340 and 412 nm. Analysis of the single-wavelength data is summarized in Figure 3A. It was found that three fairly well-resolved kinetic relaxations ($1/\tau_1 > 1/\tau_2 > 1/\tau_3$) are adequate to describe the system. Interestingly, over the DHT concentration range studied, $1/\tau_1$ has nearly linear (or nonsaturating) dependence on the concentration of DHT, $1/\tau_2$ has a hyperbolic (or saturating) dependence, and $1/\tau_3$ has no concentration dependence.

The reaction of OXA with $\alpha_2\beta_2$ was investigated at 412, 480, and 325 nm with final OXA concentrations ranging from 0.15 to 3.25 mM. As was found for DHT, the OXA reaction occurs via three kinetic relaxations. The rates and amplitudes of these relaxations ($1/\tau_1 \geq 1/\tau_2 > 1/\tau_3$) were determined by computer fitting (eq 1), and the dependencies with respect to OXA concentration are summarized in Figure 3B. These dependencies indicate kinetic relaxations that are typical of a tightly coupled system (Bernasconi, 1976) where both $1/\tau_1$ and $1/\tau_2$ exhibit hyperbolic (or saturating) dependencies on the concentration of OXA. Tight coupling occurs when $1/\tau_1$ and $1/\tau_2$ are of comparable magnitude, i.e., only 2–5-fold difference.

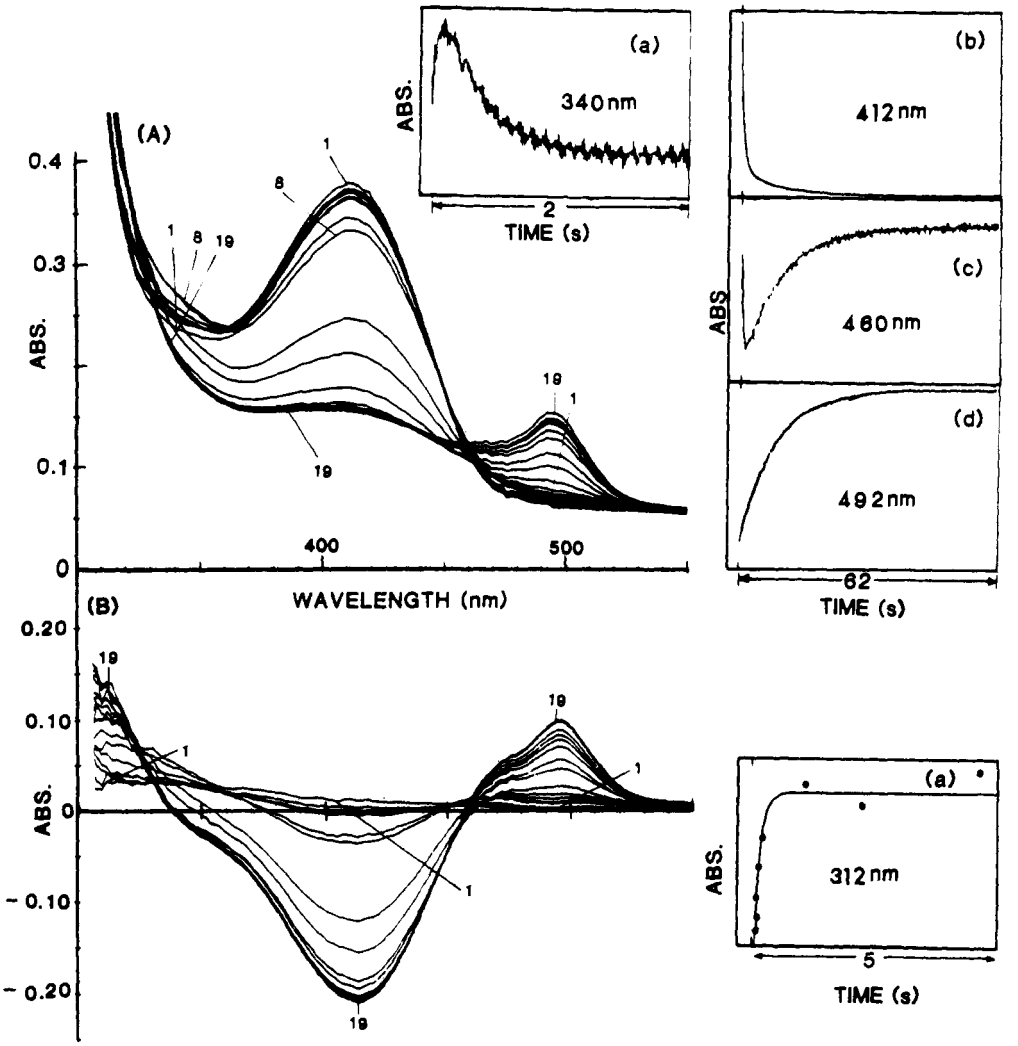

FIGURE 1: (A) Rapid-scanning spectra for the reaction of tryptophan synthase with 2,3-dihydrotryptophan in 0.1 M potassium phosphate, pH 7.8 at 22 °C. Total scan time was 68 s. Concentrations after mixing are 30 μM $\alpha\beta$ protomer and 0.5 mM DHT. The internal aldimine, λ_{max} 412 nm, completely disappears with only a small increase in quinonoid at 492 nm. The complex rise and fall at about 340 nm indicates formation and decay of an intermediate. (Inset) Representative single-wavelength stopped-flow time courses at 340 (a), 412 (b), 460 (c), and 492 nm (d) of tryptophan synthase and DHT. Conditions after mixing are 30 μM $\alpha\beta$ protomer and 1 mM DHT in 0.1 M potassium phosphate, pH 7.8 at 22 °C. Stopped-flow time courses were also collected and analyzed at substrate final concentrations of 0.25, 0.5, 1.0, 2.0, and 4.0 mM (data not shown). (B) Difference spectra calculated from the RSSF spectra presented in (A). Difference spectra were computed as $[(\text{scan})_t - (\text{scan})_0]$. Note that more than 50% of the increase at 312 nm is complete before there is any significant increase at 492 nm. Thus, the 312-nm spectral band must represent a different intermediate species rather than a second electronic transition of the 492-nm spectral band. The difference spectra have been base-line corrected for lamp drift during the experiment. The inset shows the 312-nm reaction time course reconstructed from the RSSF data.

As will be shown below, the interpretation of these two kinetic relaxations is less straightforward because both $1/\tau_1$ and $1/\tau_2$ depend on the four rate constants k_1, k_{-1}, k_2, and k_{-2} in a complex way.

Kinetic Isotope Studies on the Reaction of $\alpha_2\beta_2$ with α-^{1}H- and α-^{2}H-Substituted 2,3-Dihydrotryptophan. Transient kinetic studies were carried out to compare the effects of ^{2}H substitution for the α-^{1}H of DHT on the reaction with $\alpha_2\beta_2$. When DHT, ranging in concentration from 0.2 to 4.0 mM, is mixed with the $\alpha_2\beta_2$ complex, no change in rates or amplitudes is found (data not shown).

Discussion

2,3-Dihydrotryptophan (DHT) and oxindolyl-L-alanine (OXA) previously have been shown to be potent inhibitors of tryptophan synthase (Phillips et al., 1984, 1985). The transient kinetic studies of these reaction intermediate analogues were undertaken to further investigate the mechanism of enzyme inhibition with the expectation that new insight about tryptophan synthase catalysis would be forthcoming. The long-wavelength absorption maxima of the steady-state spectral bands formed by DHT or OXA are somewhat red-shifted in comparison to other tryptophan synthase quinonoids (Miles, 1980; Lane & Kirschner, 1981; Drewe & Dunn, 1985, 1986; Dunn et al., 1987a,b). Nevertheless, these bands have the narrow widths and shorter wavelength shoulders characteristic of quinonoids. The peak intensities are quite low, indicating these quinonoidal spectral bands account for only a small fraction of the total number of PLP species present. The quinonoids formed via attack of nucleophiles such as β-mercaptoethanol, indoline, aniline, or hydroxylamine on the α-aminoacrylate intermediate yield spectral bands with apparent extinction coefficients in the range 30 000–50 000 M^{-1} cm^{-1} (Miles, 1979; Dunn et al., 1987b). Since the fraction of enzyme bound in this form was not known in previous work, the extinction coefficients were not estimated. However, in this paper, approximate extinction coefficients of some intermediates have been determined as follows. First, from the transient kinetic data presented, apparent rate constants were calculated. Then computer simulations were carried out to

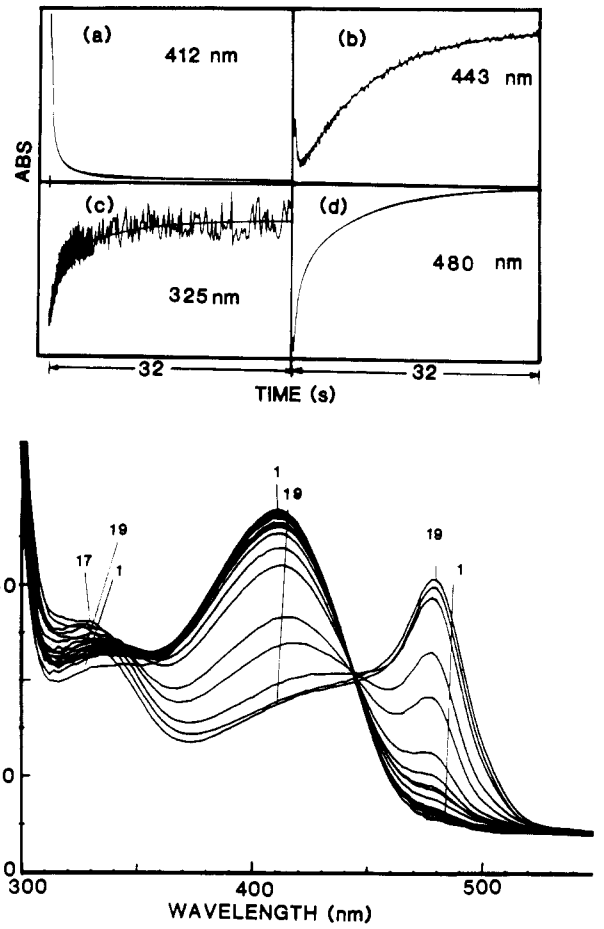

FIGURE 2: RSSF spectra showing the pre-steady-state spectral changes for the reaction of $\alpha_2\beta_2$ with oxindolyl-L-alanine. Total scan time is 62 s. Concentrations after mixing are 30 μM $\alpha\beta$ protomer and 0.5 mM OXA in 0.1 M potassium phosphate, pH 7.8 at 22 °C. The internal aldimine, λ_{max} 412 nm, decreases as the quinoidal band at 480 nm increases. (Inset) Representative single-wavelength stopped-flow time courses at 412 (a), 443 (b), 325 (c), and 480 nm (d) for the reaction of tryptophan synthase with oxindolyl-L-alanine. Conditions after mixing are 30 μM $\alpha\beta$ protomer in 0.1 M potassium phosphate, pH 7.8 at 22 °C. SWSF data was collected and analyzed at final OXA concentrations of 0.18, 0.45, 0.9, 1.8, and 3.6 mM.

test the proposed mechanisms of the enzyme interaction with substrate analogues. With a given mechanism and estimates of the specific rate constants for individual steps, the Runge–Kutta program generates time courses for enzyme-bound intermediates that are normalized with respect to relative concentrations. It is then possible to determine the concentration percentage of the intermediate with respect to total enzyme (see Materials and Methods). By use of the experimental optical density of an intermediate and fraction percent, an approximate extinction coefficient can be determined.

Pathway of the Reaction of $\alpha_2\beta_2$ with DHT. The theoretical number of relaxations possible is always equal to the number of states minus one (i.e., one for each step). If states are present at concentrations below the level of detection, some of the relaxations will not be observed. Since three phases are detected in the SWSF kinetic studies with DHT, there are no fewer than three steps in the reaction. The following mechanism (eq 2) shows the minimum number of intermediates for a linear sequence of transformations.

$$E + DHT \underset{k_{-1}}{\overset{k_1}{\rightleftharpoons}} A \underset{k_{-2}}{\overset{k_2}{\rightleftharpoons}} B \underset{k_{-3}}{\overset{k_3}{\rightleftharpoons}} C \qquad (2)$$

Since $1/\tau_1$ and $1/\tau_2$ are much greater in magnitude than $1/\tau_3$, the reaction steps characterized by $1/\tau_1$ and $1/\tau_2$ equilibrate much more rapidly and are essentially independent

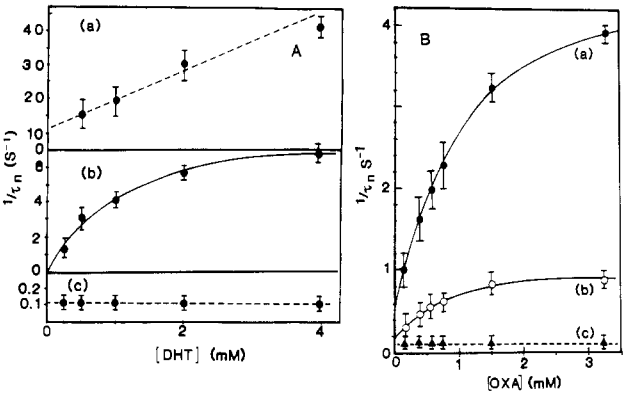

FIGURE 3: (A) Dependence of $1/\tau_n$ on DHT concentration. First-order rate constants ($1/\tau_n$) determined from the best fit of SWSF in the reaction of $\alpha_2\beta_2$ with DHT (Figure 1A) are plotted as a function of [DHT]. $1/\tau_1$ (curve a) shows a linear dependence on substrate concentration, $1/\tau_2$ (curve b) shows a hyperbolic dependence, and $1/\tau_3$ (curve c) shows no dependence. Since $1/\tau_2$ increases with increasing [DHT], a nonsequential mechanism is ruled out. (B) Dependence of $1/\tau_n$ on OXA concentration. First-order rate constants ($1/\tau_n$) determined from the best fit of SWSF data in the reaction of $\alpha_2\beta_2$ with OXA (Figure 2) were plotted as a function of [OXA]. $1/\tau_1$ (curve a) and $1/\tau_2$ (curve b) are both hyperbolic and separated in magnitude only about 5-fold. This behavior is characteristic of a tightly coupled system. $1/\tau_3$ (curve c) shows no concentration dependence.

of the reaction step(s) characterized by $1/\tau_3$. The following branched mechanism (eq 3) is also possible:

$$E + DHT \underset{k_{-1}}{\overset{k_1}{\rightleftharpoons}} A \begin{cases} \overset{k_2}{\underset{k_{-2}}{\rightleftharpoons}} B \\ \overset{k_3}{\underset{k_{-3}}{\rightleftharpoons}} C \end{cases} \qquad (3)$$

However, neither of the following branched mechanisms (eq 4 and 5) are capable of fitting the kinetic and spectral data.

$$E + DHT \begin{cases} \overset{k_1}{\underset{k_{-1}}{\rightleftharpoons}} A \overset{k_3}{\underset{k_{-3}}{\rightleftharpoons}} C \\ \overset{k_2}{\underset{k_{-2}}{\rightleftharpoons}} B \end{cases} \qquad (4)$$

$$E + DHT \begin{cases} \overset{k_1}{\underset{k_{-1}}{\rightleftharpoons}} A \overset{k_2}{\underset{k_{-2}}{\rightleftharpoons}} B \\ \overset{k_3}{\underset{k_{-3}}{\rightleftharpoons}} C \end{cases} \qquad (5)$$

Equation 4 requires that the magnitude of $1/\tau_2$ decrease with increasing substrate concentration (Hammes, 1982), while eq 5 implies that species B is on a different pathway from species C. Neither agrees with experimental observation.

Relaxation Kinetics for the Reaction of $\alpha_2\beta_2$ with DHT. Since all experiments were run with $[DHT]_0 \gg [\alpha_2\beta_2]$, the pseudo-first-order approximation is valid, and any relaxations should be single exponential in form. On the basis of concentration dependencies (Figure 3A), it is clear that $k_1[DHT]$, $k_{-1} > k_2$, $k_{-2} > k_3$, k_{-3} and that the first step equilibrates more rapidly than the second and the second equilibrates more rapidly than the third.

Expressions consistent with the behavior of the three observed kinetic phases are given in eq 6–8 [derivations are in Bernasconi (1976) pp 32 and 44],

$$1/\tau_1 = k_{-1} + k_1[DHT] \qquad (6)$$

$$1/\tau_2 = k_{-2} + k_2\left[\frac{[DHT]}{[DHT] + k_{-1}/k_1}\right] \qquad (7)$$

$$1/\tau_3 = k_{-3} + \frac{k_3(k_{-1}/k_1[DHT])(K_2)}{1 + k_{-1}/k_1 + (k_{-1}/k_1)(K_2)} \qquad (8)$$

where $K_2 = [\bar{B}]/[\bar{A}]$.

Table I: Rate Constants for the Reactions of DHT and OXA with Tryptophan Synthase[a]

substrate	k_1 (s^{-1} M^{-1})	k_{-1} (s^{-1})	k_2 (s^{-1})	k_{-2} (s^{-1})	k_3 (s^{-1})	k_{-3} (s^{-1})
DHT[b]	8.3×10^3	11.5	6	0.1	0.01	0.1
OXA[c]	2×10^3	0.35	0.5	0.34	0.01	0.01

[a] Reactions were run in potassium phosphate buffer (0.1 M), pH 7.8 at 22 °C. [b] Relaxation rate constants have been determined for the system

$$E = DHT \underset{k_{-1}}{\overset{k_1}{\rightleftharpoons}} \underset{(A)}{ES} \underset{k_2}{\overset{k_{-2}}{\rightleftharpoons}} \underset{(B)}{E_{GD}} \underset{k_{-3}}{\overset{k_3}{\rightleftharpoons}} \underset{(C)}{E_{Aex}} \overset{fast}{\rightleftharpoons} \underset{(D)}{E_Q}$$

which is described by eq 6, 7, and 9 (see text). Structures of intermediates are shown in Scheme I; for assignments, see Discussion. [c] Relaxation rate constants have been determined for the system

$$E + OXA \underset{k_{-s}}{\overset{k_s}{\rightleftharpoons}} \underset{}{ES} \underset{k_{-GD}}{\overset{k_{GD}}{\rightleftharpoons}} \underset{(X)}{E_{GD}} \underset{k_{-2}}{\overset{k_2}{\rightleftharpoons}} \underset{(Y)}{E_{Aex}} \underset{k_{-3}}{\overset{k_3}{\rightleftharpoons}} \underset{(Z)}{E_Q}$$

which is described by equations 9, 14, and 15 (see text). k_1 and k_{-1} are the apparent rate constants for the formation of E_{GD} from E and OXA and, therefore, are functions of k_s, k_{-s}, k_{GD}, and k_{-GD}. Note that since ES does not accumulate in the OXA system, k_S[OXA], $k_{-2} < k_{GD}$ and k_{-GD}. Structures of intermediates are shown in Scheme I; for assignments, see Discussion.

For the special case of $k_{-3} > k_3$, eq 8 simplifies to eq 9:

$$1/\tau_3 \simeq k_{-3} \tag{9}$$

In agreement with Figure 3A, eq 6 predicts a linear increase of $1/\tau_1$ with increasing DHT concentration with intercept k_{-1} and slope k_1, eq 7 predicts a hyperbolic increase of $1/\tau_2$ with intercept k_{-2} and an asymptote ($k_2 + k_{-2}$), and eq 8 predicts a concentration-independent behavior for $1/\tau_3$ for the special case where $k_{-3} \gg k_3$ (eq 9). The best-fit values of the rate parameters obtained by fitting the data from Figure 3A to eq 6, 7, and 9 are listed in Table I.

Absence of a Kinetic Isotope Effect. There is no detectable primary isotope effect when α-^{2}H-substituted DHT is reacted with $\alpha_2\beta_2$ (data not shown). If abstraction of an α-H were rate-limiting, then substitution of α-^{2}H for α-^{1}H should result in a primary isotope effect, i.e., a slower observed rate. There are at least two plausible explanations for not detecting an isotope effect. If the formation of the quinonoid occurs in $1/\tau_3$ via abstraction by a basic group, E–B: at the active site, then since $1/\tau_3 \simeq k_{-3}$, solvent exchange to replace E–⊕B–^{2}H with E–⊕B–^{1}H would mitigate any isotope effect. Thus, k_{-3} will reflect reprotonation of the DHT quinonoid with ^{1}H derived from solvent, not ^{2}H. Alternatively, the formation of the quinonoid might occur as a sequence of four steps with the formation of species C followed by a more rapid equilibration to species D, as shown in eq 10 and 11.

$$E + DHT \underset{k_{-1}}{\overset{k_1}{\rightleftharpoons}} A \underset{k_{-2}}{\overset{k_2}{\rightleftharpoons}} B \underset{k_{-3}}{\overset{k_3}{\rightleftharpoons}} C \overset{fast}{\rightleftharpoons} D \tag{10}$$

$$E + DHT \underset{k_{-1}}{\overset{k_1}{\rightleftharpoons}} A \begin{array}{l} \overset{k_2}{\rightleftharpoons} B \\ \underset{k_{-3}}{\overset{k_3}{\rightleftharpoons}} C \overset{fast}{\rightleftharpoons} D \end{array} \tag{11}$$

Since it is unlikely that an absorption maximum of 492 nm is anything other than a quinonoid, let alone a less conjugated intermediate, a third possibility, that no quinonoidal intermediate is formed, can be excluded.

Computer Modeling of the DHT Mechanism. With the calculated rate constants of Table I, the validity of the proposed mechanism can be further tested by simulations of the kinetic time courses. Figure 4 shows a set of digital computer simulations of single-wavelength time courses that are virtually identical with the observed single-wavelength time courses (viz., insets to Figure 1). The rate of decrease of enzyme (E) correlates to the time trace at 412 nm (inset to Figure 1A), the formation and decay of species A to the 340-nm trace, and the monophasic increase of species C to the 492-nm time trace. If the reaction pathway occurs via eq 10, then D would follow a time course identical with that shown for C. The appearance of species B is not seen in the single-wavelength studies at 412, 340, 492, or 460 nm, but is observed in the increase in absorbance around 312 nm seen in the RSSF difference spectra (Figure 1B).

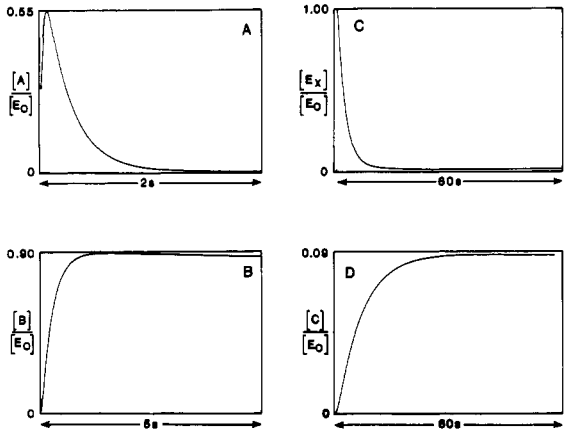

FIGURE 4: Computer simulations of SWSF traces modeled from the DHT mechanism. Simulations were calculated for the reaction of 4 mM 2,3-dihydrotryptophan with 13.3 μM $\alpha\beta$ protomer. By use of the calculated rate constants listed in Table I, the time course for the reaction is modeled as a three-step sequence, E + DHT $\rightleftharpoons$ A $\rightleftharpoons$ B $\rightleftharpoons$ C. The digital computer simulations of the kinetic time courses for each species were carried out using the fourth-order Runge–Kutta approximation algorithm. (A) Simulated time course for intermediate A. Compare with the 340-nm single-wavelength trace shown in the inset to Figure 1A. (B) Simulated time course for intermediate B, the "missing" intermediate. Compare with the 312-nm single-wavelength shown in the inset to Figure 1B. (C) Simulated time course for the native enzyme. Compare with the 412-nm single-wavelength trace shown in the inset to Figure 1A. (D) Simulated time course for intermediate C. Compare with the 492-nm single-wavelength trace shown in the inset to Figure 1A.

The relative concentrations of these species over time calculated in these simulations are shown in Figure 6A, where the computer simulations are based on the rate constants listed in Table I for 4 mM DHT and 13 μM $\alpha_2\beta_2$. At 58.8 ms, the concentration of species A reaches a maximum value, which corresponds to 53.6% of the total concentration of β sites, and then decays to a final (equilibrium) percentage of 1.45%. At equilibrium, the relative concentrations of enzyme-bound intermediates are 0.54% internal aldimine (E), 1.45% species A, 87.1% species B, and 8.69% species C (or D if the reaction pathway occurs via eq 10).

Chemical Structures of Species Formed in the Reaction of $\alpha_2\beta_2$ with DHT. If the assignment of the 492-nm band to a quinonoid species is correct, then it is reasonable to expect that the reaction of DHT with $\alpha_2\beta_2$ involves at least four interconverting species: the Michaelis complex (ES), the *gem*-diamine intermediate (E_{GD}), the external aldimine (E_{Aex}), and the quinonoid (E_Q) (Scheme I).

The structure of species A is very likely the noncovalent Michaelis complex. Because the UV–visible spectral properties are similar to those of the internal aldimine of native D-serine dehydratase, a transient intermediate in transimination is identified as a Michaelis complex (Federiuk & Shafer, 1983). The dipolar ionic form of the internal aldimine in aspartate

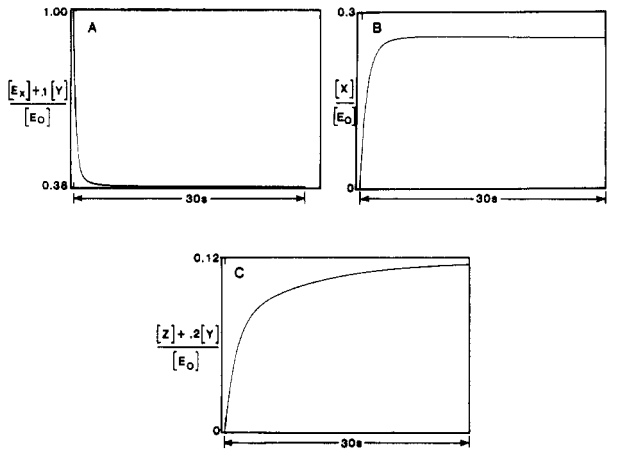

FIGURE 5: Computer simulations of SWSF traces modeled from the OXA mechanism. Simulations are of single-wavelength stopped-flow traces for the reaction of OXA with tryptophan synthase. By use of the calculated rate constants listed in Table I for 0.15 mM OXA and 30 μM $\alpha\beta$ protomer, the time course for the reaction is modeled as a three-step sequence, E + OXA $\rightleftharpoons$ X $\rightleftharpoons$ Y $\rightleftharpoons$ Z. (A) Simulated time course for the native enzyme and intermediate Y. Compare with the single-wavelength trace at 412 nm shown in the inset to Figure 2. (B) Simulated time course for intermediate X. Compare with the single-wavelength trace at 325 nm shown in the inset to Figure 2. (C) Simulated composite time course for intermediates Y and Z. Compare with the single-wavelength trace at 480 nm shown in the inset to Figure 2.

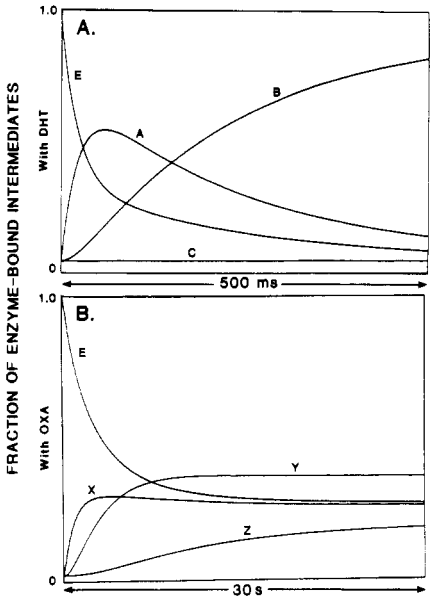

FIGURE 6: (A) Computer simulations of the formation and decay of the enzyme-bound species formed in the reaction of 4 mM DHT with 13.3 μM $\alpha\beta$ protomer over the first 500 ms of reaction. The individual extinction coefficients are normalized to show the relative concentrations of enzyme intermediates over time. (B) Computer-simulated time courses for the formation and decay of enzyme-bound species for the reaction of 0.15 mM OXA with 30 μM $\alpha\beta$ protomer over the first 30 s of reaction.

aminotransferase, with an absorption maximum at 362 nm, appears to be the active form (Torchinsky, 1986); therefore, the 360-nm spectral band detected in the reaction of 2-methylaspartate with aspartate aminotransferase has been postulated to be the absorption maximum of a Michaelis complex.

In the reaction of DHT with $\alpha_2\beta_2$, the transient changes detected during τ_1 could represent small changes in the extinction coefficient of the internal aldimine and/or redistribution of the relative amounts of preexisting PLP species as

Scheme I

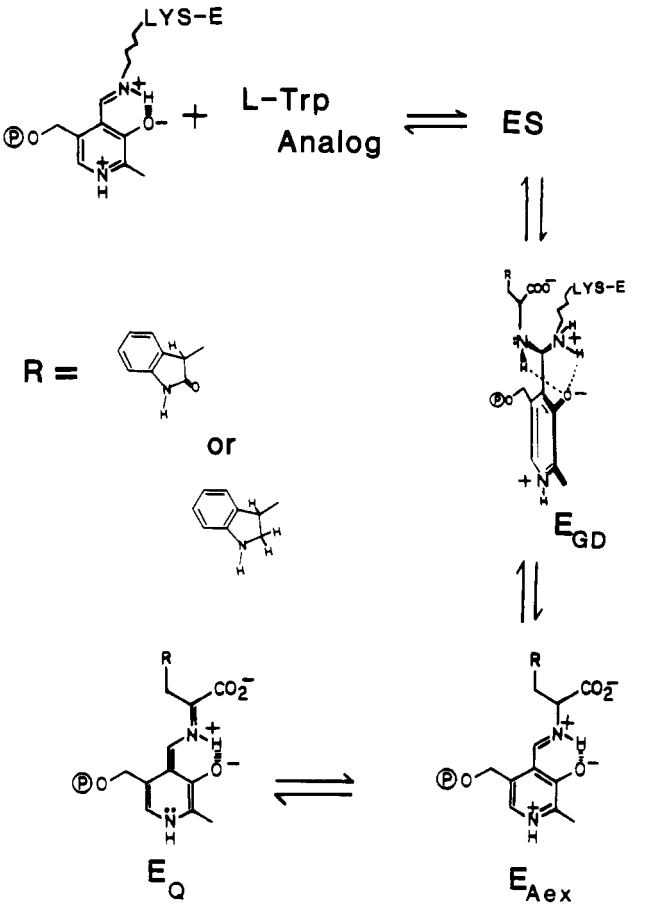

a consequence of DHT binding. These species could be the enolimine and ketoenamine tautomers of the internal aldimine.

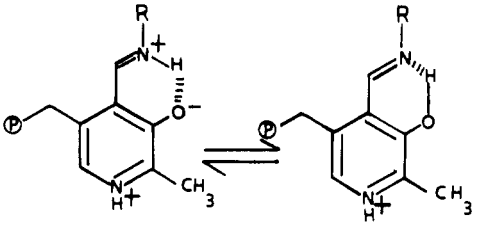

(12)

ionic tautomer (ketoenamine) neutral tautomer (enolimine)

In neutral aqueous solution, Schiff bases of PLP derived from amines with $pK_a > 7$ yield a dark yellow color characterized by an absorption band at 413–418 nm that represents the ionic ketiminium ion tautomer (Davis & Metzler, 1972; Metzler et al., 1980). In organic solvents, which may mimic the hydrophobic environment of the enzyme active site (Yang et al., 1975), the absorption maximum of model PLP Schiff bases is blue-shifted to 330–340 nm (Metzler et al., 1980). This blue shift is attributed to the neutral enolimine tautomer that Metzler et al. argue is present as a minor species in aqueous solution and can be detected as a shoulder at 330 nm. A redistribution of ketoenamine and enolimine tautomers could alter the ratio of 340- and 412-nm absorbance, thus accounting for the detection of τ_1 at these wavelengths. In glycogen phosphorylase, the enolimine form (the neutral tautomer) predominates and the λ_{max} is located at 330 nm (Johnson et al., 1970). The enolimine tautomer becomes more stable as the basicity of the amino group from which the Schiff base was derived decreases (Kallen et al., 1985).

Either species C (eq 2) or a species D rapidly formed from species C (eq 10) must be the quinonoidal (carbanionic) in-

termediate (E_Q, Scheme I). Both the bandshape and the position of the absorption maximum at 492 nm are characteristic of a quinonoidal species. The calculated extinction coefficient is $\epsilon_{492} = 37\,400\ M^{-1}\ cm^{-1}$. Typical estimates of the molar absorptivities of quinonoidal species range from 30 000 to 63 000 $M^{-1}\ cm^{-1}$; a value of 41 000 $M^{-1}\ cm^{-1}$ was determined for a quinonoid formed by the PLP enzyme, serine hydroxymethylase (Ulevitch & Kallen, 1977).

The chemical structure of species B, with a proposed absorption maximum at ≤312 nm, is most reasonably assigned to the *gem*-diamine (tetrahedral) intermediate (E_{GD}, Scheme I). Previously, tetrahedral (or *gem*-diamine) intermediates have not been rigorously identified in tryptophan synthase–substrate reactions (Miles, 1986); but tetrahedral intermediates have been seen in fluorescence and absorbance stopped-flow studies of many other PLP-requiring enzymes, including serine transhydroxymethylase (Schirch, 1975), and in model studies (Tobias & Kallen, 1975). An absorption maximum of ≤312 nm is consistent with the assignment of B as a tetrahedral species. In the reactions of glycine and of 3(*S*)-2,3-H_2-5-fluoro-DHT with $\alpha_2\beta_2$, similar bands with $\lambda_{max} \sim 330$ nm have been reported (Miles et al., 1986; Dunn et al., 1987; Houben and Dunn, unpublished results). It is likely that these also are tetrahedral species. If this assignment is correct, then at equilibrium the *gem*-diamine intermediate accounts for ~87% of the enzyme-bound PLP species present.[2]

Pathway for the Reaction of $\alpha_2\beta_2$ with OXA. As with DHT, conditions were chosen such that $[OXA]_0 \gg [\alpha_2\beta_2]$, and, again as with DHT, three phases were observed. The kinetic behavior of the OXA system is best rationalized by the pathway given in eq 13. However, extension of this pathway to include

$$E + OXA \underset{k_{-1}}{\overset{k_1}{\rightleftharpoons}} X \underset{k_{-2}}{\overset{k_2}{\rightleftharpoons}} Y \underset{k_{-3}}{\overset{k_3}{\rightleftharpoons}} Z \qquad (13)$$

one more species formed rapidly from Z (viz., eq 10) or the branched mechanism depicted in eq 3 are also possible pathways.

Relaxation Kinetics for the Reaction of $\alpha_2\beta_2$ with OXA. In view of the hyperbolic concentration dependencies for both $1/\tau_1$ and $1/\tau_2$ (Figure 3B), it is clear that two of the relaxations ($1/\tau_1$ and $1/\tau_2$) are tightly coupled and that k_1[OXA], k_{-1}, k_2, $k_{-2} > k_3$, k_{-3}. Therefore, $1/\tau_1$ and $1/\tau_2$ can be treated independently of $1/\tau_3$. When there is strong mutual coupling such as that exhibited by the OXA system, the equations for $1/\tau_1$ and $1/\tau_2$ are mathematically complex expressions, dependent on the four rate constants k_1, k_{-1}, k_2, and k_{-2}. In order to determine the specific rate coefficients, the following relationships between the kinetic relaxations are useful (Bernasconi, 1976, p 28):

$$1/\tau_1 + 1/\tau_2 = k_1[OXA] + k_{-1} + k_2 + k_{-2} \qquad (14)$$

and

$$(1/\tau_1)(1/\tau_2) = k_1(k_2 + k_{-2})[OXA] + (k_{-1}k_{-2}) \qquad (15)$$

Equations 14 and 15 predict that plots of $1/\tau_1 + 1/\tau_2$ and $(1/\tau_1)(1/\tau_2)$ versus OXA concentration will yield straight lines. If eq 14 and 15 adequately describe the first two relaxations, then with accurate values for the slopes and y intercepts it is possible to extract values for k_1, k_{-1}, k_2, and k_{-2} from these plots. Since $1/\tau_3$ shows no dependence on OXA concentration, the special case of eq 9, where $1/\tau_3 \simeq k_{-3}$, applies.

In principle, determination of the specific rate constants is straightforward. However, when the magnitudes of $1/\tau_1$ and $1/\tau_2$ are not well resolved, it is difficult to obtain precise values for the individual rate constants. With this caveat, Table I lists the best-fit values of the rate constants obtained from the slopes and intercepts of Figure 3B.

Computer Modeling of the OXA System. The calculated rate constants of Table I were fitted to eq 13, and simulated time courses were generated. Unlike the well-resolved spectral bands of the intermediates detected in the reaction of DHT with $\alpha_2\beta_2$, the spectral bands of the OXA intermediates are obviously overlapping. In the RSSF data (Figure 2), the spectral bands at 412 and 480 nm are both overlapped by a broad band centered around 440 nm (compare the base lines of Figures 1A and 2). Therefore, in order to simulate the observed single-wavelength time courses for the OXA system, it is useful to construct curves that are a composite of more than one species. Figure 5A, which models the trace at 412 nm (inset to Figure 2), is a composite of the formation and decay of both species Y and E. Figure 5B describes the absorption increase at 325 nm over time of species X, and Figure 5C is a composite of the predicted time courses for both species Z and Y at 480 nm. Parameter constants used are $[\alpha_2\beta_2]$ = 30 μM, [OXA] = 0.15 (or 1.5 mM). The extinction coefficient of the external aldimine[3] is set at $\epsilon_{440} \simeq 7500\ M^{-1}\ cm^{-1}$.

By use of the calculated rate constants, the computer-generated relative concentrations of tryptophan synthase OXA intermediates (over a 30-s time scale) have been plotted in Figure 6B. With an OXA concentration of 1.5 mM, the equilibrium concentrations of the various enzyme species are 4.4%, species E (internal aldimine); 37.1%, species X; 55%, species Y; and 5.1%, species Z.

Chemical Structures of Species Formed in the Reaction of OXA with $\alpha_2\beta_2$. As with DHT, the reaction of OXA with $\alpha_2\beta_2$ should involve the intermediate pathway depicted in Scheme I. The absorption maximum at 325 nm and the estimated extinction coefficient of 4500 $M^{-1}\ cm^{-1}$ indicate species X is probably a tetrahedral (*gem*-diamine) intermediate (see discussion of DHT intermediates; E_{GD} in Scheme I). These UV–visible spectral characteristics are similar to those of the *gem*-diamine intermediate formed in the reaction between DHT and $\alpha_2\beta_2$. The corresponding DHT species has an absorption maximum at ≤312 nm.

Species Z must be the quinonoidal intermediate (E_Q in Scheme I). Both the shape and the position (480 nm) of the long-wavelength band are characteristic of a quinonoidal structure. The calculated extinction coefficient (assuming species Y also contributes to the change in absorbance measured at 480 nm) is 50 000 $M^{-1}\ cm^{-1}$, a value somewhat higher than the 37 000 $M^{-1}\ cm^{-1}$ value assigned to the quinonoidal

[2] Since tryptophan synthase can catalyze the turnover of PMP to PLP (Miles, 1987), the bleached intermediates could also be species with tetrahedral C-4′ carbons.

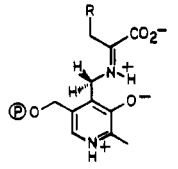

However, such a species results from the protonation of the C-4′ carbon in the quinonoidal intermediate. In the case of tryptophan synthase interactions with either OXA or DHT, the bleached intermediate occurs before the formation of the quinonoid (cf. insets C and D in Figure 1A and insets B and D in Figure 2); hence, this kinetic sequence argues against a sp^3 C-4′ species.

[3] The extinction coefficient for the external aldimine is approximated from studies of L-serine and β_2 (Miles, 1979; Drewe & Dunn, 1985). Since the neutral tautomer of the aldimine will have an absorption maximum at a shorter wavelength, the estimated extinction coefficient of the external aldimine at 440 nm is probably high.

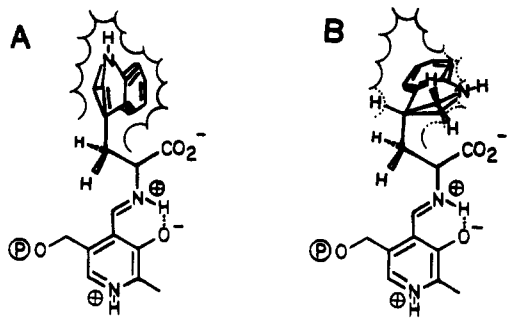

FIGURE 7: Representation of steric constraints (hypothetical) at the indole ring subsite of the β-subunit catalytic site. In (A), the subsite conformation provides a van der Waals surface (solid arcs) complementary to the indole moiety of the L-Trp Schiff base. In (B), due to the sp^3 configuration of C-3, the same subsite conformation would make unfavorable van der Waals contacts (···) with the 2,3-dihydroindole ring moiety of the DHT Schiff base.

band of DHT. And finally, the chemical structure of species Y, with a proposed absorption maximum centered at ~440 nm, is likely to be the external aldimine (E_{Aex} in Scheme I).

Steric Constraints and Conformation Change during Catalysis. In the synthesis of L-Trp from L-Ser and indole, the interconversion of β-subunit chemical intermediates occurs in a series of $sp^2 \rightleftharpoons sp^3$ interconversions at six different atoms of the reacting molecules. These atoms are the C-4′ of PLP, N-ϵ of Lys 87, C-3 of indole, and the N-α, C-α and C-β of the amino acid (L-Ser and/or L-Trp). These changes in bonding hybridization must cause large changes in the relative positions of atoms of the reacting amino acid, the indole moiety, and the PLP ring during catalysis. It is unlikely that a single-site conformation could accommodate all these structures. Consequently, it seems likely that the interconversion of these covalent intermediates is accompanied by obligatory changes in site conformation. Such conformational changes would facilitate the structural and electronic changes in the reacting substrates and cofactor. This picture of catalysis predicts that ground-state energies of intermediate states and activation energies for intermediate interconversion will be sensitive to structural alterations in substrate analogues such as DHT and OXA.

If the "bleached" intermediates detected in the reactions of DHT and OXA with $\alpha_2\beta_2$ are correctly identified as tetrahedral (*gem*-diamine) adducts, then the accumulation of these intermediates as the *most stable species* on the DHT and OXA pathways is a remarkable departure from the behaviors of the natural substrates (L-Ser and L-Trp). The *gem*-diamine species have not been detected as transient intermediates in the L-Ser or L-Trp reactions (Lane & Kirschner, 1981, 1983; Drewe & Dunn, 1985). Since the *gem*-diamines are obligatory intermediates for these reactions, decay rates must exceed the very fast formation rates. In contrast, the DHT and OXA *gem*-diamines are characterized by slow formation rates and even slower decay rates. The most remarkable structural difference between L-Trp and DHT or OXA is the geometry of the ring C-3 atom. All of the DHT and OXA intermediates retain the sp^3 configuration at C-3. The quinonoid with structure I is the only L-Trp intermediate expected to exhibit sp^3 hybridization at C-3. Therefore, only the DHT and OXA quinonoids should bind properly to the same enzyme conformation that binds the corresponding L-Trp quinonoid with sp^3 C-3 (viz., structure I). Because all other β-subunit conformations are designed to accommodate structures with sp^2 rather than sp^3 hybridization at the indole ring C-3 position (viz., Figure 7), there will be a "misfit" between the indole substrate and the 2,3-dihydroindole moiety of DHT or the oxyindole moiety of OXA for all the other intermediates. This misfitting will bring about a different set of interactions between enzyme site and reacting analogue (compare parts A and B of Figure 7) with the result that both the relative thermodynamic stabilities and the activation energies for interconversion of intermediates are changed. The enhanced stability of the DHT and OXA *gem*-diamines is the most striking manifestation of the steric and electronic constraints imposed by the site on the DHT and OXA systems.

Registry No. DHT, 103128-79-6; OXA, 16008-59-6; tryptophan synthase, 9014-52-2.

REFERENCES

Bernasconi, C. F. (1976) in *Relaxation Kinetics*, Academic, New York.

Davis, L., & Metzler, D. E. (1972) *Enzymes (3rd Ed.) 7*, 33–74.

Drewe, W. F. (1984) Dissertation, University of California, Riverside.

Drewe, W. F., & Dunn, M. F. (1985) *Biochemistry 24*, 3978–3979.

Drewe, W. F., & Dunn, M. F. (1986) *Biochemistry 25*, 2494–2501.

Dunn, M. F., Bernhard, S. A., Anderson, D., Copeland, A., Morris, R. G., & Roque, J.-P. (1979) *Biochemistry 18*, 2346–2354.

Dunn, M. F., Dietrich, H., MacGibbon, A. K. H., Koerber, S. C., & Zeppezauer, M. (1982) *Biochemistry 21*, 354–363.

Dunn, M. F., Aguilar, V., Drewe, W. R., Jr., Houben, K., Robustell, B., & Roy, M. (1987a) *Indian J. Biochem. Biophys. 24*, 44–51.

Dunn, M. F., Roy, M., Robustell, B., & Aguilar, V. (1987b) in *Proceedings of the 1987 International Congress on Chemical and Biological Aspects of Vitamin B_6 Catalysis* (Korpela, T., & Christen, P., Eds.) pp 171–181, Birkhauser, Basel.

Federiuk, C. S., & Shafer, J. A. (1983) *J. Biol. Chem. 258*, 5372–5378.

Hammes, G. G. (1982) in *Enzyme Catalysis and Regulation*, pp 180–181, Academic, New York.

Johnson, G. F., Tu, J.-I., Bartlett, M. L., & Graves, D. J. (1970) *J. Biol. Chem. 245*, 5560–5568.

Kallen, R. G., Korpela, T., Martell, A. E., Matsushima, Y., Metzler, C. M., Metzler, D. E., Morozov, Y. V., Ralston, I. M., Savin, F. A., Torchinsky, Y. M., & Ueno, H. (1985) in *Transanimases* (Christen, P., & Metzler, D., Eds.) pp 37–109, Wiley, New York.

Koerber, S. C., MacGibbon, A. K. H., Dietrich, H., Zeppezauer, M., & Dunn, M. F. (1983) *Biochemistry 22*, 3424–3431.

Lane, A. N., & Kirschner, K. (1981) *Eur. J. Biochem. 120*, 379–387.

Lane, A. N., & Kirschner, K. (1983) *Eur. J. Biochem. 129*, 571–582.

Metzler, C. M., Cahill, A., & Metzler, D. E. (1980) *J. Am. Chem. Soc. 102*, 6075–6082.

Miles, E. W. (1979) *Adv. Enzymol. Relat. Areas Mol. Biol. 49*, 127–186.

Miles, E. W. (1980) in *Biochemical and Medical Aspects of Tryptophan Metabolism* (O. Hayaishi, Ed.) pp 137–147, Elsevier/North-Holland Biomedical, Amsterdam.

Miles, E. W. (1986) in *Vitamin B_6 Pyridoxal Phosphate* (Dolphin, D., et al., Eds.) Vol. B, pp 253–310, Wiley, New York.

Miles, E. W. (1987) *Biochemistry 26*, 597–603.

Miles, E. W., & Phillips, R. S. (1985) *Biochemistry 24*, 4695.
Miles, E. W., Phillips, R. S., Yeh, H. J. C., & Cohen, L. A. (1986) *Biochemistry 25*, 4240–4249.
Phillips, R. S., Miles, E. W., & Cohen, L. A. (1984) *Biochemistry 23*, 6228–6234.
Phillips, R. S., Miles, E. W., & Cohen, L. A. (1985) *J. Biol. Chem. 260*, 14665–14670.
Schirch, L. V. (1975) *J. Biol. Chem. 250*, 1939–1945.
Tobias, P. S., & Kallen, R. G. (1975) *J. Am. Chem. Soc. 97*, 6530–6539.
Torchinsky, Y. M. (1986) in *Vitamin B_6 Pyridoxal Phosphate* (Dolphin, D., et al., Eds.) Vol. B, pp 169–222, Wiley, New York.
Turner, P. D., Loughrey, H. C., & Bailey, C. J. (1985) *Biochim. Biophys. Acta 832*, 280–287.
Ulevitch, R. J., & Kallen, R. G. (1977) *Biochemistry 16*, 5350–5354.
Yang, I. Y., Harris, C. M., Metzler, D. E., Korytnyk, W., Lachmann, B., & Potti, P. P. G. (1975) *J. Biol. Chem. 250*, 2497–2499.

^{31}P NMR Studies of the Structure of Cation–Nucleotide Complexes Bound to Porcine Muscle Adenylate Kinase†

Bruce D. Ray,‡ Paul Rösch,§ and B. D. Nageswara Rao*,‡

Department of Physics, Indiana University–Purdue University at Indianapolis (IUPUI), P.O. Box 647, Indianapolis, Indiana 46223, and Abteilung Biophysik, Max-Planck Institut für Medizinische Forschung, Jahnstrasse 29, 6900 Heidelberg, West Germany

Received March 16, 1988; Revised Manuscript Received July 6, 1988

ABSTRACT: The paramagnetic effects on the spin-relaxation rates of ^{31}P nuclei in complexes of porcine muscle adenylate kinase with ATP, GTP, GDP, and AMP were measured in the presence of two dissimilar activating paramagnetic cations, Mn(II) and Co(II), to examine the structures of the enzyme-bound complexes. Experiments were performed exclusively on enzyme-bound complexes to limit contributions to observed relaxation rates to two exchanging complexes (with and without cation). Measurements were made at three frequencies, 81, 121.5, and 190.2 MHz, and as a function of temperature in the range 5–30 °C to determine the effect of exchange on the observed relaxation rates. Relaxation rates in the E·MnATP, E·MnGTP, and E·MnGDP complexes were shown to be exchange-limited and therefore without structural information. Relaxation rates for the complexes E·CoATP, E·CoGTP, and E·CoGDP were shown to depend on Co(II)–^{31}P distances. Inability to precisely estimate spectral densities arising from electronic relaxation of Co(II) restricts calculations of Co(II)–^{31}P distances in these complexes to upper and lower limits. At the center of these limits, the Co(II)–^{31}P distances of β-P and γ-P in E·CoATP and E·CoGTP, and of β-P (E·CoGDP), are in the range 3.1–3.5 Å appropriate for the first coordination sphere. For all these complexes, the corresponding distance for α-P is appreciably larger in the range 3.9–4.5 Å. In the quaternary complex, E·MnGDP·AMP, while the ^{31}P relaxation rates of α-P and β-P (GDP) were exchange-limited, that for ^{31}P in AMP was only partially exchange limited at 121.5 MHz [because of the longer Mn(II)–^{31}P distance] as evidenced by its frequency dependence and an activation energy of 4 kcal/mol. The ability to measure structure-dependent ^{31}P relaxation rates for AMP in the quaternary complex with both Mn(II) and Co(II) at all the frequencies allowed approximate estimates of the lifetime and correlation time for the Mn(II) complex. On this basis a value of 5.9 Å appears appropriate for the Mn(II)–P(AMP) distance in the complexes E·MnGDP·AMP and E·CoGDP·AMP.

Adenylate kinase (EC 2.7.4.3) catalyzes the reversible reaction[1]

$$\text{MgATP} + \text{AMP} \rightleftharpoons \text{MgADP} + \text{ADP} \qquad (1)$$

The enzyme is most abundant in tissues, such as muscle, in which the energy turnover is considerable (Noda, 1973) and is essential for production of adenine nucleotides beyond the monophosphate. Kinetic and NMR experiments have detected two distinct substrate binding sites, one of which binds MgATP and MgADP while the other is specific for uncomplexed AMP and ADP (Noda, 1958; Rhoads & Lowenstein, 1968; Hamada & Kuby, 1978; Nageswara Rao et al., 1978). GTP and MgGTP are known to bind at the MgATP site with reasonable affinity (Price et al., 1973). In contrast, however, the AMP site is highly specific for adenine nucleotides.

There is continuing debate about the positions of the two substrate binding sites on adenylate kinase despite the fact that

† This work was supported in part by grants from the NSF (DMB 8309120 and DMB 86 08185). The NTC-300 NMR spectrometer at IUPUI was purchased with partial support from NSF (PCM 80 18725). Collaboration between research groups in Indianapolis and Heidelberg, West Germany, was partially supported by NATO Award RG86/1030. The Purdue Biochemical Magnetic Resonance Laboratory is supported by NIH Grant RR01077. A preliminary version of some of this work was presented at the Biophysical Society Meeting in New Orleans, LA, in Feb 1987.

* Author to whom correspondence should be addressed.
‡ Indiana University–Purdue University at Indianapolis.
§ Max-Planck Institut für Medizinische Forschung.

[1] Abbreviations: ATP, adenosine 5′-triphosphate; ADP, adenosine 5′-diphosphate; AMP, adenosine 5′-monophosphate; GTP, guanosine 5′-triphosphate; GDP, guanosine 5′-diphosphate; DTT, dithiothreitol; EDTA, ethylenediaminetetraacetic acid; Hepes, *N*-(2-hydroxyethyl)-piperazine-*N*′-2-ethanesulfonic acid; E·M·S, enzyme–metal–substrate; E·S, enzyme–substrate; NTP, nucleoside 5′-triphosphate; NDP, nucleoside 5′-diphosphate; EPR, electron paramagnetic resonance; NMR, nuclear magnetic resonance; CD, circular dichroism.

0006-2960/88/0427-8669$01.50/0